1996ApJ...470...63F

THE ASTROPHYSICAL JOURNAL, 470:63–77, 1996 October 10
© 1996. The American Astronomical Society. All rights reserved. Printed in U.S.A.

A BALLOON-BORNE MILLIMETER-WAVE TELESCOPE FOR COSMIC MICROWAVE BACKGROUND ANISOTROPY MEASUREMENTS

D. J. FIXSEN,[1] E. S. CHENG,[2] D. A. COTTINGHAM,[3] W. C. FOLZ,[2] C. A. INMAN,[4] M. S. KOWITT,[2]
S. S. MEYER,[4] L. A. PAGE,[5] J. L. PUCHALLA,[2] J. E. RUHL,[4] AND R. F. SILVERBERG[2]
Received 1995 November 12; accepted 1996 April 30

ABSTRACT

We report on the characteristics and design details of the Medium Scale Anisotropy Measurement telescope, a millimeter-wave, balloon-borne experiment that measures anisotropy in the cosmic microwave background radiation on 0°.5 angular scales. The gondola is capable of maintaining orientation to 2′ rms and determining absolute pointing to 2′.5 accuracy during a one-night flight. Emphasis is placed on the optical and pointing performance as well as the weight and power budgets. We also discuss the total balloon/gondola mechanical system. The pendulation from this system is a ubiquitous perturbation on the pointing system. A detailed understanding in these areas is needed for developing the next generation of balloon-borne instruments.

Subject headings: balloons — cosmic microwave background — instrumentation: miscellaneous — telescopes

1. INTRODUCTION

The Medium Scale Anisotropy Measurement (MSAM) is designed to measure variations in the 2.7 K cosmic microwave background radiation (CMBR; White, Scott, & Silk 1994) on 0°.5 angular scales. The telescope we are describing was used for three flights (from 1992 through 1995) during the first phase of the project (MSAM1). For these measurements we used a bolometric receiver with four channels at 5.7, 9.3, 16.5, and 22.6 cm^{-1} (170, 280, 500, and 680 GHz, or 1.75, 1.08, 0.61, and 0.44 mm) with approximately 1.5 cm^{-1} bandwidth in each channel. The results of the first flight (MSAM1-92, 1992 June 4–5) are reported by Cheng et al. (1994) and Kowitt et al. (1996). This flight observed an arc at a declination of 82°. Preliminary results from the second flight (MSAM1-94, 1994 June 1–2) are reported by Cheng et al. (1996) and Inman et al. (1996). This flight duplicated the sky coverage of the first flight in order to confirm the detection of anisotropy in the CMBR. Analysis for the third flight (MSAM1-95, 1995 June 1–2) is in progress. This last flight doubled our sky coverage, adding an arc at a declination of 80°.5 at roughly the same right ascensions. Small improvements were made between flights and are summarized in Table 1.

The MSAM1 configuration of the experiment was retired after MSAM1-95. We plan to use the same telescope and gondola with a new radiometer for a series of measurements (MSAM2) beginning in 1996. Other instruments designed for similar observations are described in Fischer et al. (1992), Meinhold et al. (1993), and de Bernardis et al. (1994).

Both the gondola and the radiometer for MSAM1 have flown before. The gondola was used with a different telescope and radiometer to map the Galactic plane (Hauser et al. 1984). The radiometer had been flown three times for the Far InfraRed Survey (FIRS; Meyer, Cheng, & Page 1991; Ganga et al. 1993, 1994) that confirmed the anisotropy detection from NASA's *Cosmic Background Explorer* (*COBE*) mission (Bennett et al. 1994). The cryostat, bolometers, and filter bandpasses are discussed in Page (1989), Page, Cheng, & Meyer (1990), and Page et al. (1994). For MSAM1, we replaced the cryogenic chopper in the FIRS configuration with a dichroic beam splitter, since internal referencing was not required, and we replaced the cold feed horn and lens with an elliptical concentrator to match the telescope optics. The only other significant modification to the radiometer was replacing the external preamplifiers before MSAM1-94. These amplifiers and associated support for the cold detector electronics are located immediately outside the cryostat at the hermetic connector for the signals, and provide the first gain stage for the signals. This change improved the noise performance and stability of the detectors, and helped to eliminate some sensitivities to microphonics and "popcorn" noise.

The main components of the instrument are shown in Figure 1. The gondola frame is attached to the balloon by a rigid tubular superstructure at the top of the gondola (MSAM1-92), or a cable system (MSAM1-94 and later). This frame supports the telemetry electronics, batteries, and pointing system mechanisms.

The entire gondola frame is controlled in azimuth by a servomechanism during flight. Two symmetrical elevation-drive motors support the telescope metering structure (the "strongback"). This structure holds all the elevation-controlled components. These include the primary mirror, the secondary mirror and chopper, the star camera(s), the cryostat and related signal electronics, the secondary magnetometer, and the gyroscope.

The gondola is operated during flight in a manner that both minimizes changes of the gondola orientation relative to the Earth and provides three levels of modulation to aid

[1] Applied Research Corporation, NASA Goddard Space Flight Center, Laboratory for Astronomy and Solar Physics, Code 685.3, Greenbelt, MD 20771.
[2] NASA Goddard Space Flight Center, Laboratory for Astronomy and Solar Physics, Code 685, Greenbelt, MD 20771.
[3] Global Science and Technology, Inc., NASA Goddard Space Flight Center, Laboratory for Astronomy and Solar Physics, Code 685, Greenbelt, MD 20771.
[4] Physics Department, University of Chicago, 5641 South Ingleside Avenue, Chicago, IL 60637.
[5] Department of Physics, Princeton University, Jadwin Hall, Princeton, NJ 08540.

© American Astronomical Society • Provided by the NASA Astrophysics Data System

1996ApJ...470...63F

TABLE 1

HARDWARE STATUS SUMMARY FOR THE MSAM1 FLIGHTS

Flight	Date	Hardware Change
MSAM1-92.....	1992 June 4–5	First flight of MSAM1
MSAM1-94.....	1994 June 1–2	Minimized area of the structure above the gondola; improved coupling to balloon flight train (jitter mechanism); tested new star camera; new warm preamplifier for the detectors
MSAM1-95.....	1995 June 1–2	New star camera; improved ground screen construction method

in the detection and removal of certain observational errors (atmospheric drifts, telescope offset drifts, sidelobe pickup, etc.). The first level is provided by a nutating secondary mirror (chopper) operating at 2 Hz (see Fig. 2, *first panel at left*). This frequency is above the $1/f$ knee ($\sim$0.5 Hz) of the detectors and front-end electronics. The detailed operation of the chopper is described below. The second level is the "scan" motion. Here the telescope azimuth is swept in a triangle wave pattern with a 1 minute period and with an amplitude matching the chopper throw. The telescope tracks sky inertial coordinates throughout this motion. The third modulation level shifts the scan center approximately every 20 minutes by the chopper throw amplitude, in the direction that restores the azimuth position to slightly east of true north (see Fig. 2, *farthest right panel*). This has the effect of placing the scan center at the extreme position of the previous scan, providing a large degree of sky position overlap.

In this paper, we concentrate on the following items: the telescope optics, the temperature of the optical elements, and the attitude control systems. We provide some crude estimates and discussion of the systematic errors involved in these measurements, mostly to motivate the design considerations. Weight and power budgets are provided, as

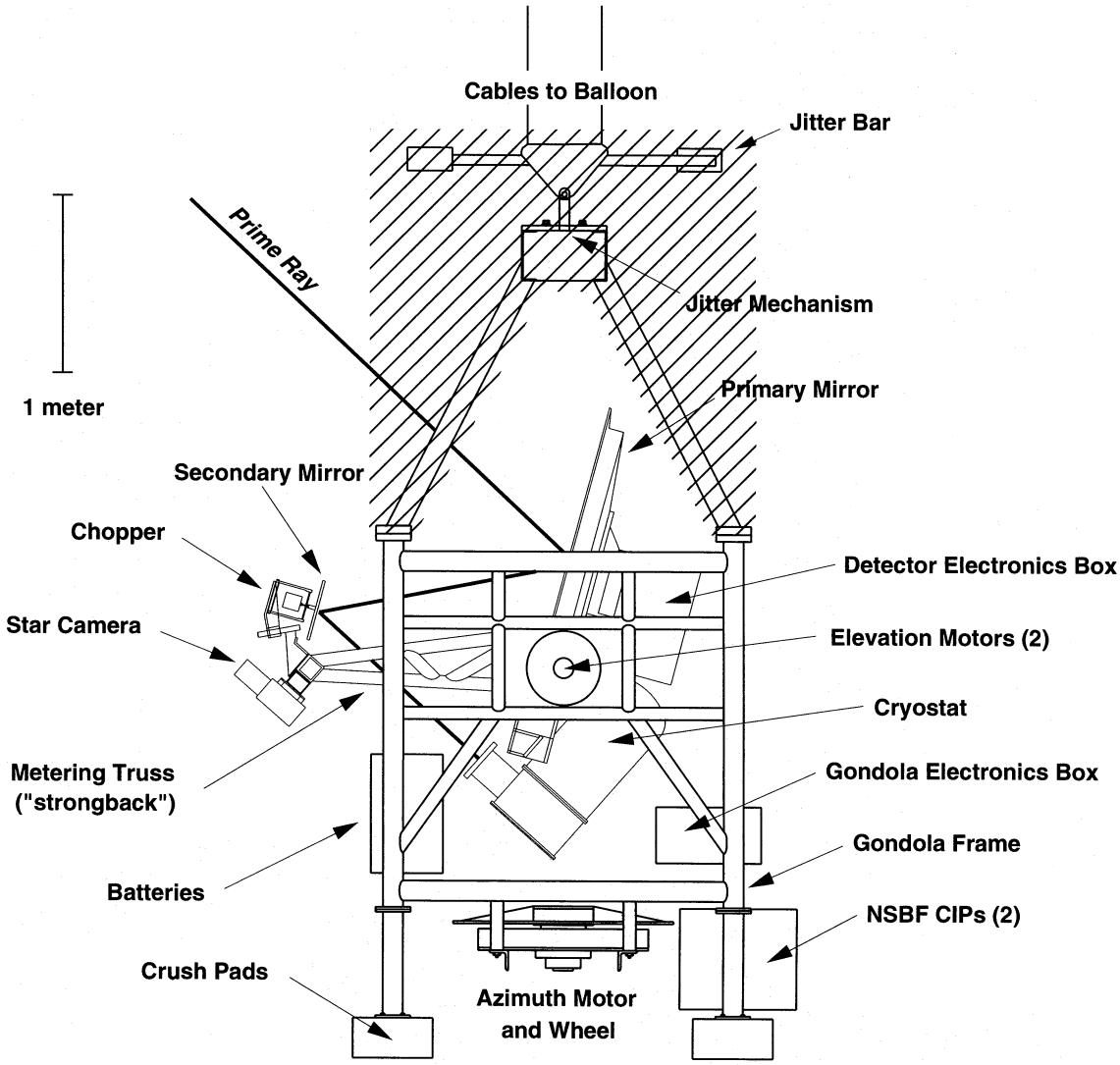

FIG. 1.—Side view of the gondola and telescope MSAM1-92 configuration. The shaded structure on top of the gondola was replaced by a wire rope cable system for MSAM1-94 and later flights. The ground shield is omitted for clarity.

© American Astronomical Society • Provided by the NASA Astrophysics Data System

1996ApJ...470...63F

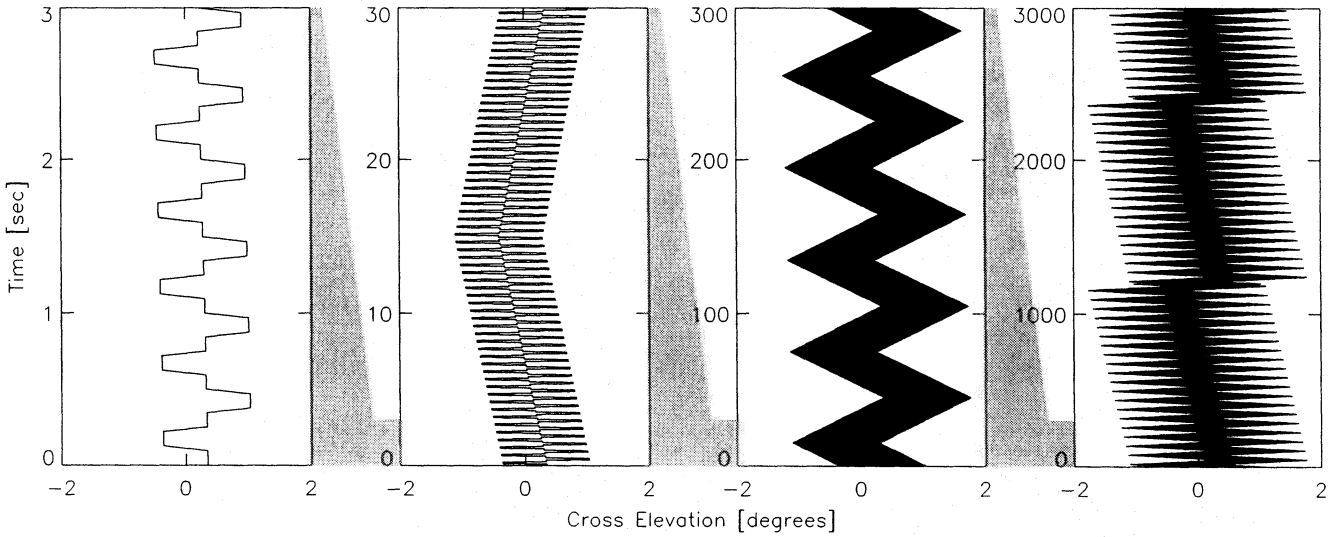

FIG. 2.—The MSAM chopping strategy. Illustration of the various levels of modulation in the instrument: secondary mirror chopper pattern (*farthest left panel*), gondola scan pattern (*middle panels*), and sky rotation (*farthest right panel*). Each panel shows the nominal position of the telescope beam as time advances vertically; successive panels increase the timescale tenfold (*as indicated by the shading*). The horizontal axes plot azimuth divided by the cosine of the elevation angle.

these are of interest for any balloon-borne instrument that must operate for many hours under battery power. This information will be useful for developing the next generation of balloon-borne instruments for CMBR measurements, such as the TopHat telescope for the top of a balloon (Cheng 1994; Kowitt et al. 1995), or large-aperture gondolas of the standard design for high-resolution observations.

2. TELESCOPE OPTICS

The optical configuration is a 1372 mm, 51° off-axis Cassegrain with a nutating secondary. The optical layout is illustrated in Figure 3. The entire telescope assembly is controlled by an altitude-azimuth mount. The effective beam size[6] is 37′, and the secondary has a ±40′ throw. The throw is in a plane 65°.2 from the beam such that (1) the center of the chop is a line of symmetry for the optical system and (2) the motion is parallel to the local horizon. While this is neither a great circle nor a line of constant elevation, the small motion makes it a good approximation to both.[7] In flight, the chopper executes a four-phase cycle in the following sequence: (1) 125 ms on the central spot, (2) 125 ms on a spot 40′ to the left, (3) 125 ms on the central spot, and (4) 125 ms on a spot 40′ to the right. These times include a 23 ms transition time. The phase of the demodulation is found by observing Jupiter, as described in Cheng et al. (1994).

This chopping cycle puts the signal information for the center relative to the edges (double difference) at 4 Hz and its odd harmonics, while the difference between the two edges (single difference) is at 2 Hz and its odd harmonics. Thus, the double- and single-difference data can be analyzed separately. These form nearly statistically independent data sets and correspond to different angular scales on the sky.

There are several critical optical parameters that can affect the reliability of the experiment. First, the offset of the instrument must be small and stable to enable making

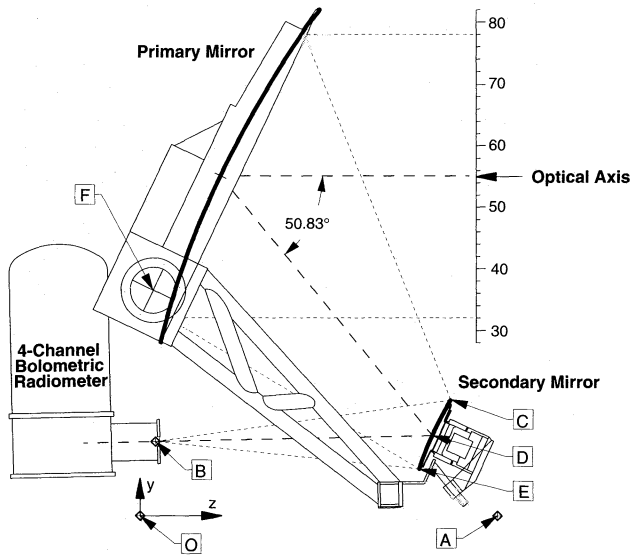


```
A (0,  0    , 58.0  )   Prime Focus
B (0, 12.0  ,  2.5  )   Secondary Focus
C (0, 18.719, 50.374)   Top of Secondary Mirror
D (0, 12.982, 47.387)   Center of Secondary Mirror
E (0,  7.612, 45.252)   Bottom of Secondary Mirror
F                       Elevation Axis
O (0,  0    ,  0    )   Origin of Primary Coordinates
```

FIG. 3.—The MSAM telescope optics. All distance units are in inches. The primary mirror surface is specified by $z = (x^2 + y^2)/4f$, $f = 58$. The secondary mirror surface is specified by $z' = a[1 + (x' + y')/b^2]^{1/2}$, $a = 14.065$, $b = 24.662$. Primed coordinates have their origin centered between the prime and secondary foci with the $+z'$-axis passing through the prime focus and $x' = x$. The chief ray is in the y-z plane. The sky beam is parallel to the z-axis. The chopper rotation axis is parallel to the line through points C and E and 0.225 inches behind it (farther from the primary mirror).

[6] Effective beam size is defined as $2 \int P\, d\Omega/(\pi \int P^2\, d\Omega)^{1/2}$, where P is the antenna response. The more traditional definition, $2(\int P\, d\Omega/\pi)^{1/2}/P(0)$, yields 28′, which is also the approximate full width at half-maximum.

[7] The motion of the optical beam on the sky is approximately in the cross-elevation direction, which is defined by a great circle perpendicular to the line of constant azimuth at the beam center. For an elevation h and a change in azimuth $\delta\theta$, the change in cross-elevation is approximately $\delta\theta/\cos h$.

© American Astronomical Society • Provided by the NASA Astrophysics Data System

1996ApJ...470...63F

precise measurements of ~ 30 μK temperature differences. This is controlled mainly by the surface emissivity of the mirrors, their thermal properties, and the symmetry of the optical paths (and thus the chopper stability). Additionally, the sidelobes of the telescope must be exceedingly small to minimize sensitivity to intensity variations in the environment (outside of the main beam). The measured performance of the MSAM1 instrument in these areas is discussed in subsequent sections.

2.1. *Primary and Secondary Mirrors and Chopper*

The off-axis parabolic primary mirror has an elliptical edge with 1372 × 1518 mm axes and a focal length of 1473 mm. It is machined from a single piece of aluminum (6061-T6) and lightened by machining 9 pockets out of the back, leaving support ribs which are 68 mm deep and 9.5 mm wide, and a 10 mm thick "skin" on the front surface, for a total weight of 75 kg. The lowest vibrational mode is 214 Hz. This mirror is fabricated on a numerically controlled milling machine with a ball mill. Appropriate stress relieving after each cut preserves its dimensional stability. After machining, the last pass on the mill is made with a polishing tool to remove the fine grooves left by the ball mill, leaving a surface finish of ~ 2 microinches (~ 0.05 μm) rms.

The secondary mirror is a convex hyperbola and has an elliptical edge with 276 × 315 mm axes. The secondary mirror is the limiting stop for the optical system. The edge of the primary mirror is not used ($\gtrsim 20$ dB attenuation relative to the center), and any excess sensitivity from the radiometer horn at large beam angles spills onto the cold sky (behind the secondary mirror). The secondary mirror design is similar to the primary mirror but on a smaller scale. Its ribs are 22 mm deep and 2.5 mm wide, and the front "skin" is 1 mm thick, for a total mass of 550 g, and a moment of inertia about the moving axis of ~ 2.6 g m^2. Its lowest vibrational mode is 342 Hz. The finish on the secondary mirror is better than the finish on the primary mirror.

To move the beam 40′ on the sky, the secondary mirror must be rotated 1°.79 about the vertical axis. A schematic diagram of this mechanism is shown in Figure 4. It is driven by a pair of Gearing & Watson GWV4 Mk II linear motors that weigh 2.5 kg each and together use 30 W when chopping. Most of the power is used to deflect the centering springs in the linear motors. The transition time is 23 ms (to 90%). The system is overdamped with a ~ 30 ms decay time. The drive signal is filtered to remove frequencies outside the mirror drive response band. It is derived from a square wave that is passed through a 4 pole low-pass Bessel filter with a 32 Hz 3 dB point. The chopping is stabilized by feedback from a linear variable differential transformer (Lucas Schaevitz E 200 LVDT) operated at 16.39 kHz modulation with a response bandwidth of 1 kHz to position, and a linear velocity transducer (Lucas Schaevitz 3L5 VT-Z LVT), operated with a 1.5 kHz bandwidth. The position sensor indicates that the chopping is stable to 4″ (on the sky) over the entire flight, both in the central position and in the amplitude of the chop. The total mass of the chopper assembly is 8 kg.

2.2. *Feed Horn*

The beam-forming horn for the system is an elliptical Winston cone concentrator cooled to 4.2 K (see Fig. 5). It is designed to concentrate light from the secondary mirror onto the feed horn throat (4.5 mm diameter) for a design étendue of 0.5 cm^2 sr. The horn is 275 mm long and has a diameter of 45.1 mm at the mouth. A detailed geometrical ray trace shows that virtually all of the radiation passing through the throat comes from the surface of the secondary mirror. Diffraction effects degrade this performance for the low-frequency channel. The diffraction is estimated by propagating 10,000 rays from a point in the throat of the Winston cone to the mouth of the Winston cone, keeping track of the phase of each ray. The pattern at the secondary mirror is then determined by integrating over the mouth of the horn for each point at the secondary mirror. This is repeated for each of 19 modes (at 6 cm^{-1}) that the horn supports in each polarization, and the result is the sum over all modes. Because the E-field varies over the mouth of the horn, the final beam is wider than simply convolving the ray trace pattern with an Airy pattern for a 45 mm circle. The diffraction calculations agree reasonably well with ground tests and laboratory measurements. Both show that $\sim 10\%$ of the radiation is from outside the secondary mirror for the 5.7 cm^{-1} channel. This fraction is less than 4% for the shorter wavelength channels.

2.3. *Radiometer*

The radiometer design and its support electronics are essentially the same as that used for the FIRS (Page 1989;

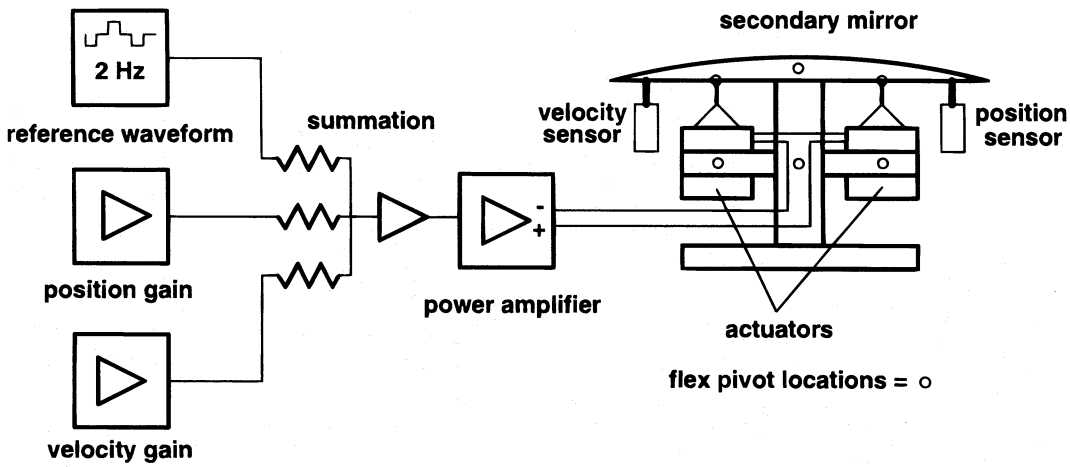

FIG. 4.—Schematic diagram of the secondary mirror chopper mechanism

© American Astronomical Society • Provided by the NASA Astrophysics Data System

1996ApJ...470...63F

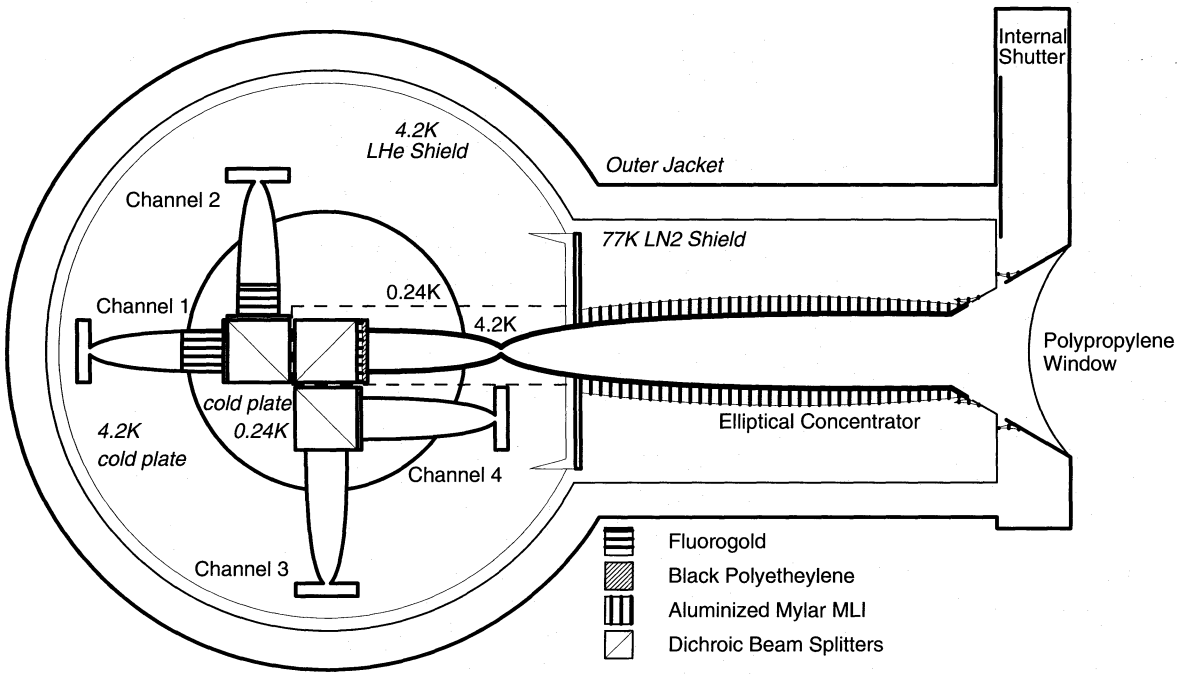

FIG. 5.—Schematic diagram of the cold optics in the radiometer. The input elliptical concentrator, its collimating horn, and the first optical block (with black polyethylene and fluorogold absorbers) are all maintained at close to 4.2 K. The rest of the optics and detectors are at 0.24 K.

Page et al. 1994). The main difference is the replacement of the cryogenic chopper with a dichroic at the first optical block (see Fig. 5) and the new feed horn discussed in the previous section.

The optical structures are made from copper (OFHC 101). These blocks support all the filter elements, provide thermal sinking to the appropriate cold stage, and enclose the 25.4 mm diameter light pipes.

The incoming beam is collimated and mid-IR filtered with black polyethylene at 4.2 K, and then split twice using capacitive grid dichroics (once at 4.2 K and once at 0.24 K) to form the four channels. Each channel has a Winston concentrator feeding a monolithic silicon bolometer (Downey et al. 1984). In front of each concentrator is a band-defining filter. The detailed passband measurements are discussed in Page et al. (1994).

The bolometer outputs are fed into cold JFET followers, and then to preamplifiers external to the cryostat. The internal wiring of the high-impedance leads is through small-gauge manganin wire that is glued inside a small, thin stainless steel tube in order to minimize microphonic pickup and to provide shielding. This arrangement creates a low thermal conductivity, rigid coaxial signal line.

All of the internal cryostat lines, including housekeeping, power, and buffered detector signals, pass through connectors manufactured by Microtech, Inc., which are potted in RF absorbing epoxy (Emerson-Cumming CR-117). These connectors are compact and reliable at cryogenic temperatures. However, their small size makes assembly somewhat challenging, especially when they are used with small-gauge stainless steel or manganin wires.

All the cryostat lines are also fed through RF π-filters at the hermetic connectors on the cryostat shell. This precaution has allowed us to make repeatable noise measurements in different environments (including that at the National Scientific Balloon Facility [NSBF], where there are frequently intentional RF transmissions of modest power). In general, we have attempted to maintain an RF attenuation between 20 and 40 dB above 1 MHz (with rolloff for higher frequencies), depending on the signal and space constraints.

A commandable shutter is included inside the cryostat vacuum jacket immediately before the feed horn. This is a copper sheet with an evaporated gold surface that covers the entire open aperture of the horn. When closed, the shutter presents a $\sim$160 K surface to the feed horn. This shutter is opened before launch and kept open for most of the flight. Near or at sunrise, it is closed to block the optical signal, but the gondola continues to execute normal scanning motion for 20 minutes. This test provides a useful confirmation that observed offsets are optical.

A backup external shutter mechanism is available for protecting the polypropylene window at the cryostat entrance aperture. This shutter places an aluminum sheet between the cryostat window and the incoming beam, and prevents a severe problem should the telescope inadvertently point at the Sun after the attitude control system is powered down. Since we need this protection only after the flight is over, the mechanism is a one-shot, spring-deployed design that is actuated by melting a pair of nylon lines.

2.4. *Alignment*

With the two mirrors and the feed horn, there is a total of 12 degrees of freedom involved in the alignment process. Each optical element is placed at its nominal design position by a machined mount, and then shimmed by measurement. In combination, these mounts allow 4 degrees of freedom: the horn can be rotated about the radiometer's vertical axis, it can be raised or lowered, the secondary mirror can be moved closer to or farther from the primary, and it can be rotated about its vertical axis. The telescope is aligned by first centering the feed horn beam on the secondary mirror by mapping the feed horn pattern at the second-

© American Astronomical Society • Provided by the NASA Astrophysics Data System

1996ApJ...470...63F

ary mirror location and shimming the position of the cryostat. Subsequently, the position of the secondary mirror is shimmed so that the center position beam is symmetrically placed on the primary mirror.

The main lobe of the beam was measured by observing both a blackbody source and a microwave source on the ground. The measured beam profile is used to verify the alignment of the telescope and to establish a reference position for the IR beam center in the CCD star camera. The final determination of the beam pattern and IR beam center position is made in-flight by observing Jupiter. The results of one such determination are shown in Figure 6. The ground-based maps agree with the flight measurements in the central lobe to 10% of the peak response, limited by the accuracy of the ground test data. There is typically a shift of approximately 10′ in cross-elevation and 5′ in elevation in beam position (relative to the camera) between the ground and flight measurements.

The large beam size makes alignment of the telescope relatively straightforward. Typical alignment requirements for the various adjustments are ~2 mm for the cryostat position and ~10 mm for the centering of the beam on the primary mirror, and these were easily achieved.

2.5. *Ground Shield*

The ground shield is a critical element that shields the radiometer input aperture, the secondary mirror, and most of the primary mirror from the Earth during observations. The shield is constructed at the launch site from foam building insulation. For MSAM1-92, a 15 m^2, 50 kg shield was constructed with foiled, polyisocyanurate fiberboard building insulation covered on the interior side with an additional 0.25 mm aluminum sheet (see Fig. 7). With the wire rope top structure for MSAM1-94, a smaller 5 m^2 shield was built using similar methods. Unfortunately, some of this foam exploded during ascent and at float altitude. The additional aluminum sheet remained, however, preserving the optical integrity of the shield. For MSAM1-95, we used unbacked closed-cell Styrofoam with an aluminum sheet on the interior side and aluminized Mylar on the outside. These materials withstood the rigors of the (night) flight environment without incident. We performed some destructive daytime tests at the end of the flight to gain some experience for future packages. Styrofoam covered with aluminized Mylar melts with only a few tens of minutes of exposure to sunlight if the aluminized side faces out.

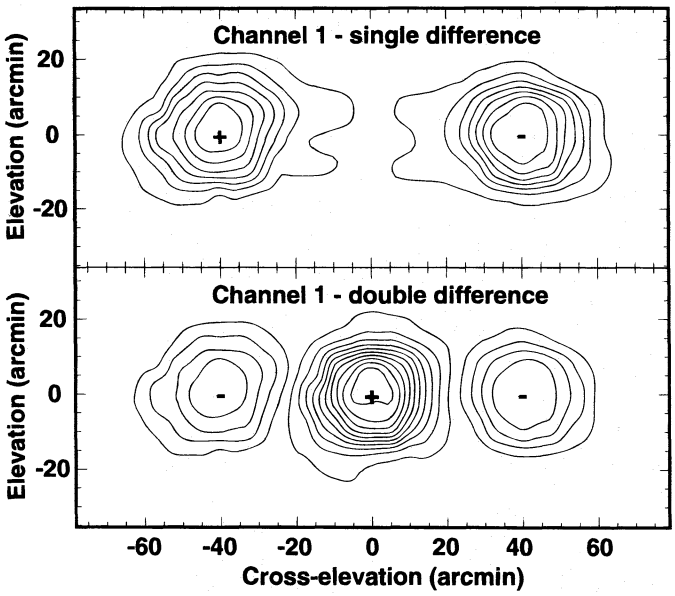

FIG. 6.—Single and double difference maps made in flight on Jupiter by the 5.7 cm^{-1} channel. The contours are at uniform linear intervals. The other channels are very similar. These data were taken by moving the gondola in a raster pattern, 1°1 peak to peak in elevation and 3° in cross-elevation. The elevation motion is in 9 steps, while the cross-elevation motion is a smooth scan. The raster represents approximately 10 minutes of data.

Two sets of tests were performed to measure the far sidelobe response of the telescope. The first, a near-field test, provides a sensitive measurement of the beam response to sources near the horizon, and helps to pinpoint "trouble spots" in the shielding and gondola structure that could potentially cause unacceptable levels of response. The second, a far-field test, maps the response of the beam as a function of angle from the main lobe as the telescope is raised in elevation.

The near-field test was done with the gondola placed in a parking lot, pointed at its nominal observing elevation of ~40°. A millimeter-wave source, placed on a tripod ~5 m from the gondola, was pointed successively at the body of the gondola, the top edge of the telescope shielding, and the gondola top support structure. This procedure was repeated at 10 positions on a circle surrounding the gondola (at 0°, 10°, 45°, 90°, 135°, 180°, 225°, 270°, 315°, and 350° azimuth).

For the MSAM1-92 flight, the near-field test was performed using an Alpha Industries 180 V 60.6 GHz diode followed by a Millitech MU3W15-01 tripler (10 μW) and a standard 21 dB horn used as the point source. Although this 182 GHz (6.07 cm^{-1}) source could only be seen in the lowest frequency channel, this channel has the most diffraction, suggesting that it would have the largest effect. We found that the solid top structure reflected some radiation (~ −55 dB) into the detector, motivating the change to the cable top structure for the later flights.

For the second and third (MSAM1-94, MSAM1-95) flights we used a 150 GHz Litton LST9423XX Gunn diode (30 mW) and a 21 dB horn as the point source for the near-field tests. With the new top structure, which was smaller and farther from the beam axis than the old structure, we found no positions with sensitivity above −75 dB.

The far-field sidelobe test was done just prior to the second flight (MSAM1-94). A 1 m on-axis Cassegrain telescope (~53 dB gain, the transmitting telescope) was placed on top of the 25 m control tower at the NSBF in Palestine, Texas, with the MSAM gondola situated 740 m away in a clearing (the "old launch pad"). The same 150 GHz Gunn diode used for the near-field tests was coupled to the transmitting telescope through a Winston concentrator at the secondary focus.

The transmitting telescope was pointed at the MSAM telescope and left in that position throughout the tests. To avoid saturating the bolometric detector in MSAM while measuring the on-axis response, it was necessary to attenuate the transmitted power by inserting microwave absorbing material in the feed optics. After the on-axis response was measured (with the MSAM telescope pointed at a low elevation near the horizon), the MSAM telescope was raised in elevation to map the response as this moved the source off axis. Once the MSAM telescope was pointed a few degrees off axis, the absorbing material was removed from

© American Astronomical Society • Provided by the NASA Astrophysics Data System

1996ApJ...470...63F

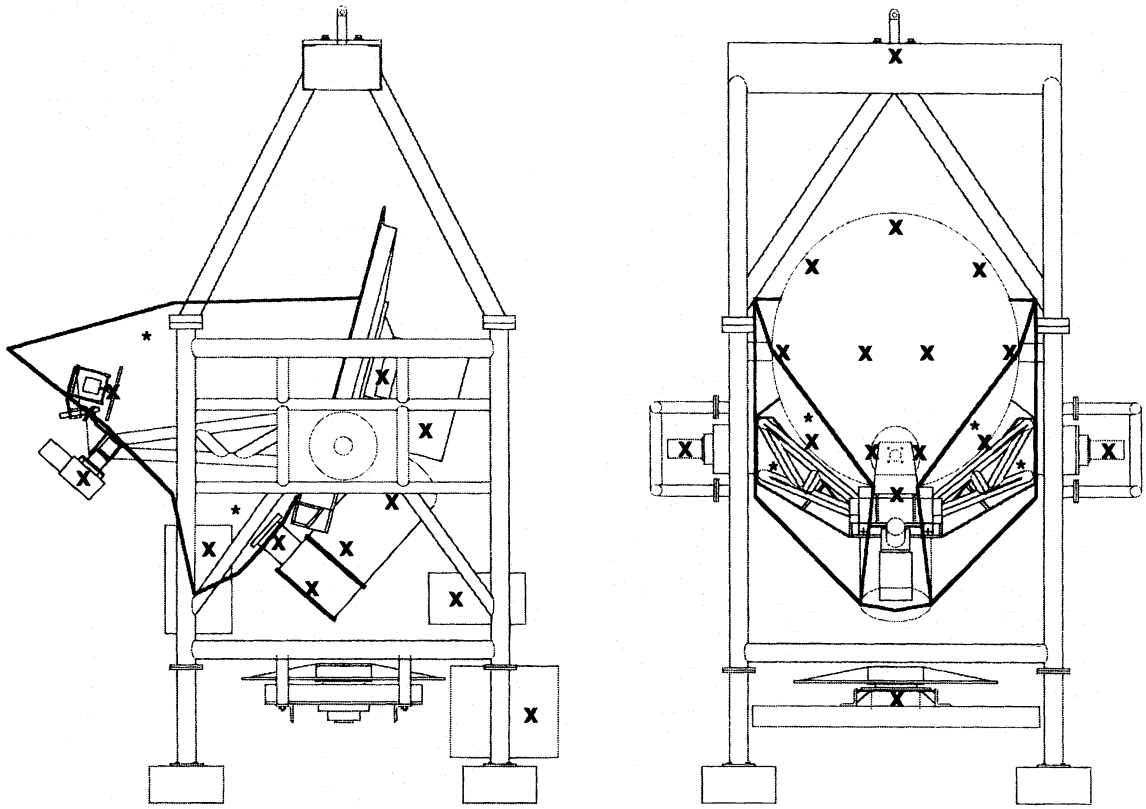

FIG. 7.—Two views of the gondola showing some thermometer locations. Many items have been omitted for clarity. The ground shield outline is shown. The asterisks show the approximate positions of the temperature sensors on the ground screens, and the crosses show the sensor locations on the other gondola components. Note that the shield hides the horn, most of the primary mirror, and the secondary mirror from the horizon and below. Diagram (*a*) shows the gondola near the nominal observing position. In (*b*) the elevation of the telescope is at a lower position to afford a clearer view of the primary mirror.

the feed optics. The removal of the material caused a change in MSAM's response, which in turn calibrated the attenuation factor of the material. This procedure provided sufficient dynamic range to map the sidelobes to roughly -100 dB, as shown in Figure 8. The uncertainty in the level of the far sidelobes relative to the main beam is roughly 3 dB, dominated by the uncertainty in calibrating the attenuating material.

The same transmitting telescope fed by a ~ 1000 K blackbody source allowed us to map the main lobe in all four channels out to ~ -25 dB. This was used as a check for beam symmetry and focus prior to flight. A similar arrangement, but using a small (0.1 m) polyethylene lens instead of the 1 m telescope, was used for the same purpose prior to the first and third flights. This setup was effective for checking the main lobe out to ~ -20 dB.

Another test before the MSAM1-94 flight measured the telescope response at elevation angles higher than the beam. The MSAM telescope was placed ~ 12 m from the edge of the control tower, and illuminated by the 150 GHz Gunn diode and 21 dB horn from the top of that tower. The telescope was positioned in the nominal flight elevation of 40° and the Gunn diode placed at 62° elevation to simulate the limb of the balloon during flight. This measurement constrains the instrument response at the edge of the balloon during nominal flight observations to be less than -55 dB. The measurement is dominated by reflections off the side of the control tower and is thus an upper limit.

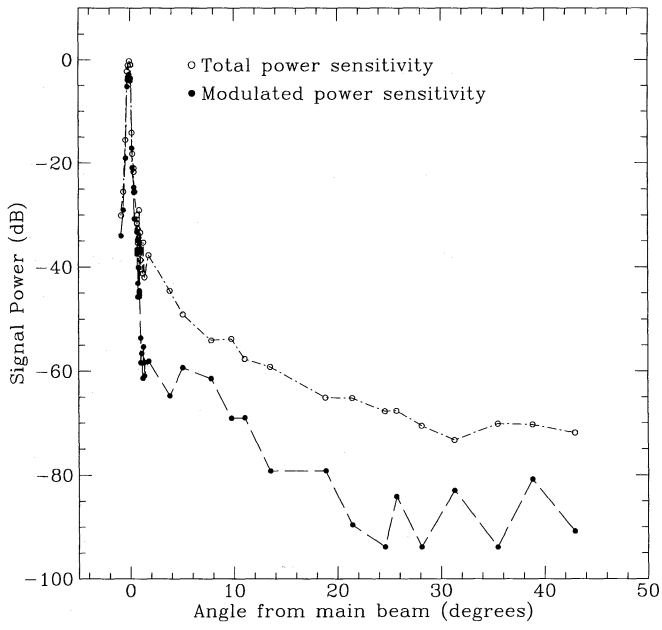

FIG. 8.—Far sidelobes as measured before the MSAM1-94 flight using a 1 m telescope for illumination. Both the total power sensitivity and the sensitivity to the component that is synchronous with the secondary mirror modulation are shown. The latter is typically a factor of 10 below the total power sensitivity. The plotted data are for a scan in the elevation direction. The horizontal axis shows the angle of the transmitter *below* the main beam in elevation.

© American Astronomical Society • Provided by the NASA Astrophysics Data System

1996ApJ...470...63F

For all of these measurements, the source was modulated at ~0.7 Hz, while the secondary was moving in its normal 3 beam pattern (at 2 Hz full cycle). We recorded both the fundamental modulation frequency and the appropriate sidebands of the secondary mirror chopper frequency, thus measuring both the chopped (synchronous with the secondary mirror modulation) and the total power sensitivities. All the numbers quoted in the text are for the chopped case unless otherwise noted. The total power sidelobe response is roughly a factor of 10 higher than the chopped response.

2.6. *Sidelobe Performance*

In-flight elevation scans are made to check obvious sidelobe sensitivities as well as the total atmospheric emission. The results of these scans for MSAM1-92 are shown in Figure 9 (after replacement of the top structure of the gondola, the subsequent flights do not show any such effect). The expected emission from the atmosphere is $T_z \csc \theta$, where T_z is the zenith temperature and θ is the zenith angle. Since the bolometers are AC coupled, we expect to see the derivative of T_z as in the channel 3 data. An anomalous feature appears in channel 1 at high elevations, probably arising from stray radiation from the top of the gondola. The antenna temperature from this source is ~4 K, an amount that is consistent with ~4% of the solid angle subtended by the ground having the −55 dB response seen in the test.[8] For MSAM1-94 and later flights, the large feature at high elevation is no longer present, consistent with the hypothesis that it was a result of reflection off the top of the gondola.

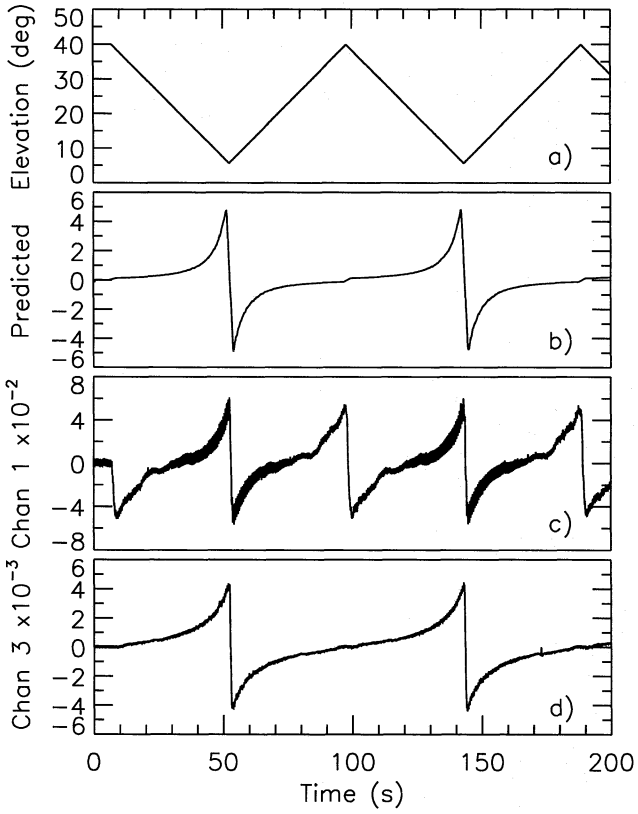

FIG. 9.—Data from the elevation scans for MSAM1-92 showing a diffraction effect in channel 1 (5.7 cm^{-1}). This effect was eliminated for subsequent flights. All plots are a function of time measured in seconds: (*a*) elevation in degrees, (*b*) predicted signal shape, (*c*) signal in channel 1, (*d*) signal in channel 3 (16.5 cm^{-1}). The feature at $t = 172$ in (*d*) is a cosmic-ray hit on the detector. The bottom three panels are plotted in linear power units on the vertical axis. The signals are AC coupled, causing the diffraction effect to appear as a double-cusped signal in channel 1.

There are three different ways in which such an effect might contaminate the data. One is by the signal induced by elevation motions (~3 mK arcmin^{-1}). While the elevation should be roughly independent of time for our observations, there may be some residual coupling between the elevation and azimuth positions arising from small misalignments of the gyroscope axes with the horizon. Ground-based measurements place an upper limit of 6′ on the misalignment, which corresponds to an upper limit of 0.′18 pitch change over the gondola scan distance (1.°5 peak to peak). The net result is a total change in observed power of ~540 μK. The secondary mirror chopping reduces this effect by at least a factor of 10 (confirmed by the elevation scan data), and the strategy of repeated measurements of the same point in the sky in the right, center, and left chopped beams reduces the effect further by at least a factor of 2. The net result from this source is conservatively estimated to be less than 30 μK.

A second contamination source is present even if the elevation stays constant. The ultimate source of the radiation (presumably the ground) is not constant, varying both in time (as the balloon floats along) and in space. The spatial correlations are not well understood, as we have only a rough idea of the far-sidelobe pattern, but tens of μK signals are possible in MSAM1-92. The change in the mechanical structure for MSAM1-94 and MSAM1-95 reduces this contribution to less than 1 μK.

This estimate is derived from the following reasoning. For MSAM1-92, we see 2 out of 30 measured far-sidelobe locations where there is a response at the level of −55 dB. Assuming that the ground emits at 300 K, this would appear as a total power of 1000 μK per point. Assuming also that the ground variations are on the order of 10%, this is reduced to 100 μK per point. Our measurements indicate that the chopped response in the far sidelobes is approximately a factor of 10 below the total power response, further reducing this number to a modulated power of 10 μK per point. On the horizon, we estimate that there are ~720 beams in azimuth by ~10 beams in elevation, making a total of 7200 beams. Taking a ratio of 2 out of 30 beams having the anomalous response, we are left with ~480 bad spots. Assuming further that these spots are not correlated produces an estimate of the total contribution as $10(480)^{1/2} = 220$ μK. Because of the scanning motion, we measure the same spot on the sky about 20 times per scan, and we measure a particular spot in three consecutive scans. This reduces the problem by another factor of ~5, leaving an obviously crude estimate of ~50 μK. For MSAM1-94 and MSAM1-95, there were no spots with a response greater than −75 dB, leading to the reduced estimate.

An upper limit on this effect can be derived from the analysis in Inman et al. (1996). In this comparison of the MSAM1-92 and MSAM1-94 flights, we find that the CMBR signal in 0.°24 × 0.°24 bins on the sky are consistent. From this, we can conclude that the sidelobe contamination is likely to be less than the noise on each of these bins. The

[8] We measured the sidelobe response while illuminating the gondola from 30 positions on the "horizon" during ground testing. These positions included all of the intuitively obvious worst-case locations. Two of these had a −55 dB response.

© American Astronomical Society • Provided by the NASA Astrophysics Data System

1996ApJ...470...63F

TABLE 2

POINTING SYSTEM SENSORS

Sensor	Roll Axis (left-right tilt)	Pitch Axis (elevation)	Yaw Axis (azimuth)
First sensor	Secondary gyro[a]	Primary gyro	Primary gyro
Second sensor.....	Magnetometer	Angle encoder	Magnetometer
Third sensor	Camera	Inclinometer	Magnetometer
Fourth sensor.....	...	Camera	Camera
First control	None	Elevation drive	Reaction wheel
Second control.....	...	Fluid pump	Jitter bearing

[a] Only on MSAM1-92 and MSAM1-95.

CMBR bins have noise of $\sim 30\ \mu$K (Rayleigh-Jeans, 1 σ). In the lowest frequency channel, this corresponds to $\sim 40\ \mu$K (thermodynamic, 2.7 K CMBR).

A third contamination source could arise from small optical misalignments that show up as an inconsistency in results when the gondola is moving toward the left or the right. We have tried to detect these effects, and the difference is less than 15 μK (95% confidence) for all channels combined. This result shows that any such bias is much smaller than the primary sky signal and can be safely ignored.

In light of some of these uncertainties, the MSAM1-94 flight covered the same sky as the MSAM1-92 flight in order to validate the observations. Both flights concentrated on an arc at $\delta = 81^\circ.8$ and $15^h < \alpha < 20^h$. Analysis results suggest that the two flights detect very similar structure, placing the best limit on any contamination to either flight (Kowitt et al. 1996; Inman et al. 1996).

3. ATTITUDE CONTROL

The telescope consists of the primary mirror, the secondary mirror, a 100 kg cryostat, and 45 kg bolometer electronics all mounted on a 140 kg supporting structure (strongback). The two-axis active control system, with damping, has feedback from a number of sensors to control pointing. The system can be organized by the control axis and sensor (see Table 2). The roll axis (and thus rotation about the optical axis) is passively controlled by the balance of the gondola. Although the balance adjustment is simple (lead bricks), we are able to level the gondola to 10′ before launch. In flight it is stable to 3′ after the swinging attenuates (~ 30 minutes after float altitude is reached).

There are a number of sensors and controls for each of the axes. Much of this redundancy is for historical reasons and would not be necessary in a new design. However, all of the sensors have proved to be valuable for detailed reconstruction of the in-flight telescope performance. A block diagram of the control system is shown in Figure 10.

3.1. *Gyroscopes*

The main gyroscope is a Teledyne Systems Model SDG-4 No. 8005304-503 two-axis rate gyroscope mounted on the strongback with the gyroscope axis aligned with the telescope optical axis to within 1°. The gyroscope is accurate to 1′, with a drift rate less than 10′ hr^{-1} after warmup and compensation. The electronics use analog components to

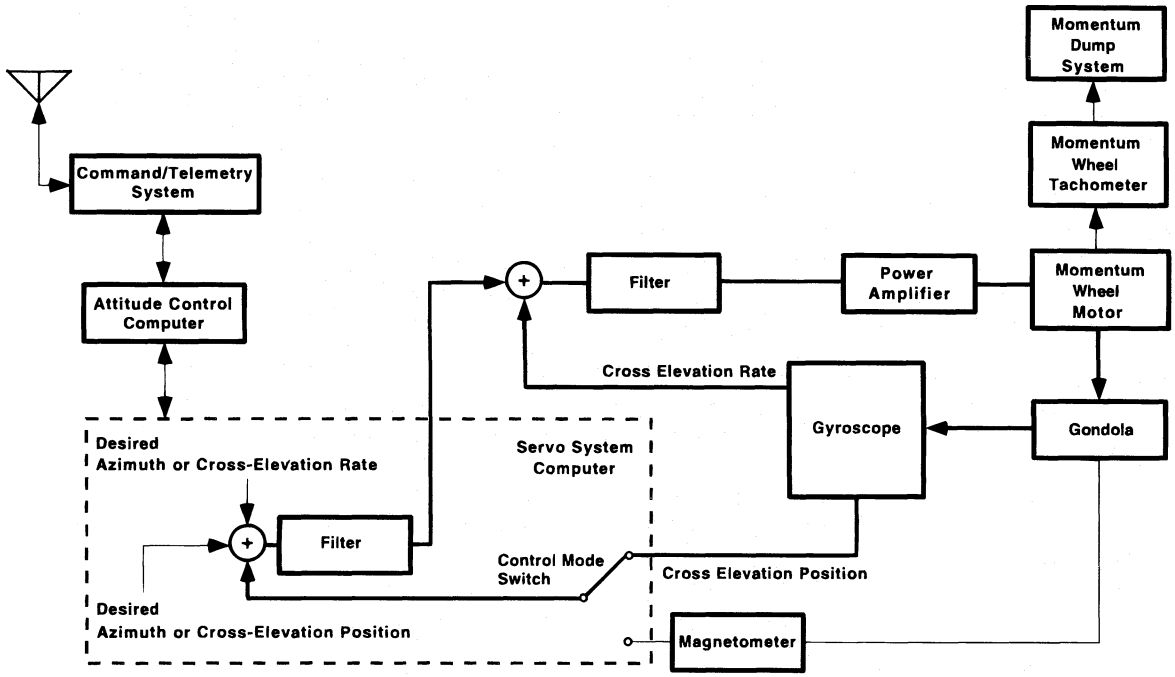

FIG. 10.—Block diagram of the azimuth attitude control system. The switch illustrates a configuration change that is available during a flight. The indicated switch setting is the nominal flight configuration. The elevation control system is somewhat simpler because a momentum dump is not required, but it is of a similar design.

© American Astronomical Society • Provided by the NASA Astrophysics Data System

1996ApJ...470...63F

integrate the signal and provide the primary pointing reference over 20 minute scan periods.

For MSAM1-92, the secondary gyroscopes are a pair of Kearfott vertical gyroscopes (model C704132001) which derive their long-term stability from gravity. These are used outside the control loops to measure the swinging of the gondola. No secondary gyroscopes were flown on MSAM1-94. On MSAM1-95, we used a surplus Pershing II, two-axis rate gyroscope (model 11502525-039) as the secondary gyroscope to monitor roll, with the goal of using it in the control loop for future flights.

3.2. *Magnetometers*

Two flux gate magnetometers are flown on the package to measure the local magnetic field. The primary magnetometer is a two-axis device that is fixed to the gondola frame. The secondary magnetometer senses three orthogonal axes and is mounted on the primary mirror support structure. The primary magnetometer was built at Goddard Space Flight Center, and the secondary magnetometer was purchased from Schoensted. The accuracy limitations in this system are the distortions of the Earth's magnetic field from moving parts of the electronics and the magnetic materials in the gondola itself, and from uncertainties in the magnetic field at float altitude. The absolute accuracy of the magnetometers is limited to about 1°, but their low weight and power consumption (<1 kg, <1 W), combined with their absolute azimuth readout, make them attractive sensors.

3.3. *Camera*

The ultimate pointing reference for MSAM1-92 is a charge injection device (CID) star camera (General Electric model 2200, 6 kg, 20 W). The 128 × 128 detector has a field of view of 8° × 8° at a resolution of 3.8 × 3.8. The camera is sensitive to wavelengths from 400 to 950 nm. With an integration time of 10 s, it detects F stars of $M_V < 5.6$ and K stars of $M_V < 5.8$. On-board processing of the images identifies the location and brightness of the stars in each frame. Because of the long integration time, the telescope must be held fixed to take a picture. This is done between scans (every 20 minutes). Only the star positions are transmitted to the ground.

For MSAM1-94, we added a second star camera (Photometrics model Star 1, 3 kg, 15 W). This 576 × 384 charge-coupled device (CCD) detector has a field of view of 9° × 6° at a resolution of ~0.9. This camera is sensitive to wavelengths from 400 to 1000 nm. With an integration time of 0.1 s, it easily detects stars of $M_V \sim 7$. Although the required integration time is short enough to take pictures at any time, the temporal registration between the camera and gyroscope data was not good enough to use these pictures except when we stopped to get a picture with the CID camera between 20 minute scans.

For MSAM1-95, we used only the Photometrics camera, and refined the time registration scheme, so that readings taken during scans can be used for pointing reconstruction. A standard V-band filter is used to improve photometry for star recognition.

3.4. *Elevation Control*

The elevation, or pitch control, is maintained by a pair of torque motors (Inland Motors model T-7203, 33 kg, 40 W peak power each). An error signal is obtained by subtracting the desired angle from the sensor angle (the sensor can be selected from the list in Table 2). This error signal is fed back with an adjustable gain and offset to the torque motors to correct the error. When the gain is too high, a mode involving the pitching of the telescope and counter-pitching of the gondola is excited. With proper adjustment, the servo has a time constant of 0.3 s and is stable to 2′, more than adequate for the 37′ beam.

The long-term stability of the pitch is perturbed by the evaporation of liquid nitrogen from the cryostat. This is compensated by a system that pumps aircraft hydraulic fluid between two tanks, one on the cryostat support structure and the other on the gondola frame. The pump speed is determined by the averaged elevation motor current, thereby working to reduce any elevation torque imbalance.

3.5. *Azimuth Control*

The azimuth, or yaw, control is similar to the elevation control. The azimuth is maintained by a torque motor identical to the pitch motors driving a momentum wheel (77 kg, 15 kg m^2) to change the angular momentum of the gondola frame. Mechanical and/or electrical biases would tend to spin up the momentum wheel so that the angular momentum is transferred to the flight train and eventually to the balloon through the "jitter" mechanism described below. The system is similar to the one discussed in Hazen, Coyle, & Diamond 1974 and Hazen 1974.

For MSAM1-92, the entire gondola was hung from a pair of bearings suspended by the flight train (see Fig. 11*a*). The jitter mechanism keeps the bearings in motion by oscillating a short shaft between the two bearings, thus maintaining dynamic friction rather than the higher static friction (stiction). The stiction is a factor of 5 higher than the dynamic friction, and the transition introduces an undesirable nonlinear response in the control system. A jitter bar (34 kg, 11 kg m^2) is added to the bottom of the flight train to provide reaction inertia for the bearing connected to the flight train rather than induce a twist in the flight train (43 N m rad^{-1}).

The jitter mechanism also transfers angular momentum to the flight train. This is done by biasing the motion of the bearing to the direction necessary to apply a torque (0–0.5 N m) to the flight train. The jitter mechanism (including motor) weighs 55 kg and uses 28 W.

For MSAM1-94 a new jitter mechanism (Fig. 11*b*) was installed. The bearings for this new jitter mechanism had a factor of ~10 less friction, and we were able to run without the oscillation and without the jitter bar. The bearings used are from Precision Consolidated Bearings, model 51212P/5.

The adjustment of the azimuth feedback is complicated by two factors. The first is the lack of information about the flight train dynamics. The bottom of the flight train is a pair of parallel cables, 0.48 m apart, and the upper part is connected to a parachute, which is in turn attached to the balloon. Neither can be treated as a rigid structure. The length of the flight train (104 m) complicates efforts to develop a ground-based test setup. In addition, the different air-damping effects on the ground and at float altitude need to be taken into account. The second complication is that, although the secondary magnetometers measure true azimuth, the gyroscope measures cross-elevation change, which is $\sim \delta\theta/\cos h$, where $\delta\theta$ is the azimuth change and h is the elevation. Hence the gain (and damping) in the feedback loop is a function of elevation when the gyroscope is used.

© American Astronomical Society • Provided by the NASA Astrophysics Data System

1996ApJ...470...63F

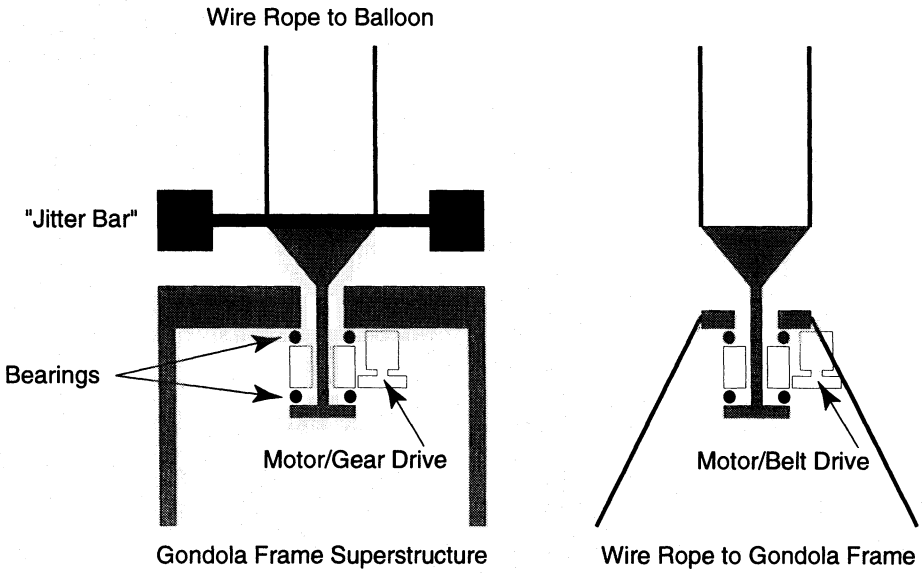

FIG. 11.—*Left:* schematic diagram of the jitter mechanism used for MSAM1-92. *Right:* schematic diagram of the corresponding improved mechanism for MSAM1-94 and later flights.

This could be corrected by the flight software but was not, since we generally operate over a small range of elevations. The azimuth time constant is 2 s, and a 0.°7 step function settles to 90% settling in 1.5 s. In flight, the azimuth error is 2′ rms, with long-term drifts of ~4′.

3.6. *Camera Results*

Absolute pointing is determined by matching images taken by the star camera against a star catalog. This fixes the position of the camera frame at the time the exposure was taken. Between pictures, position is interpolated using the gyroscope, with a small linear drift correction to make the gyroscope readings consistent with the camera pictures. This correction is typically 2′ in 20 minutes. The relative position of the camera frame and the telescope beam is fixed by a simultaneous observation of Jupiter with the camera and the telescope/radiometer. The resulting pointing is accurate to 2.′5, limited by the gyroscope drift correction. A plot of the MSAM1 pointing performance during a typical 20 minute scan is shown in Figure 12.

3.7. *Pendulation and Other Spurious Motions*

The secondary gyroscopes show regular swinging motions at several times during a flight. During some of these events, the rotational encoders in the elevation drive also show relative motion of the telescope and the gondola (in elevation). These motions are less than 10′ during observations, but can be much larger after the system has been significantly perturbed. We have constructed a simple model for understanding these motions.

The major mechanical flight components are a 1880 kg gondola, a 2300 kg balloon, a 200 kg ladder line, and 720 kg of helium gas in the balloon. Assumptions used in the calculations include a rigid spherical balloon with uniform mass distribution over the surface (130 m diameter), a rigid 104 m ladder line with uniform mass distribution, and a rigid gondola with a radius of gyration of 1 m. Prediction of the various modes of pendulation is straightforward, but the model is obviously too simple. The interaction of these components with the surrounding air is an important aspect that cannot be ignored. Rather than construct a detailed model, we lump this interaction into a single approximation: the amount of air effectively coupled to the balloon. One might reasonably expect that this amount will be between zero and the total mass displaced by the balloon (5100 kg). We ignore damping, even though the effective Q-values are only of order 30. We expect that some of this dissipation is within the moving air, with the remainder caused by flexing within the structures. Even with this simple model, we get three modes that match the observed motions (see Fig. 13).

The lowest frequency mode is one in which the entire flight assembly swings back and forth as a unit. The predicted period for this mode is between 26 and 34 s, depending on the coupling to the air. In the early part of the flight an oscillation was observed with a period of 28 s, which damps in about 30 minutes. Using the model described above, this corresponds to a coupled air mass of 15% of the total displacement of the balloon.

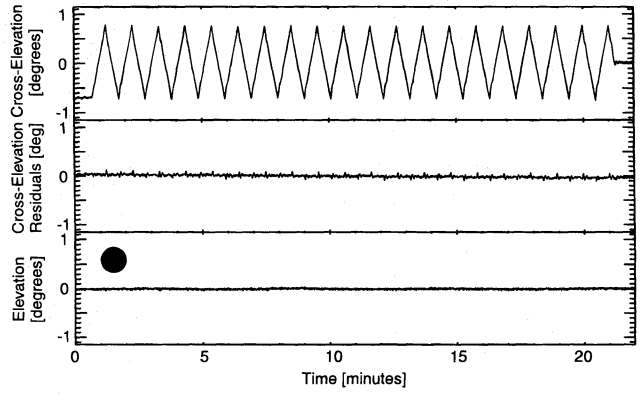

FIG. 12.—In-flight cross-elevation and elevation during a 20 minute scan (as measured by the gyroscope integrated position signal). The top panel is the cross-elevation signal. The middle panel shows the cross-elevation residuals after removing the desired (sawtooth) scan motion. The bottom panel shows the elevation position signal, which should be constant over the plotted range. These coordinates are fixed relative to the sky. This pattern is repeated by joining the flat regions of cross-elevation at the edges of the plot. All three plots are on the same scale with arbitrary zero points. The circle shows our nominal beam size.

© American Astronomical Society • Provided by the NASA Astrophysics Data System

1996ApJ...470...63F

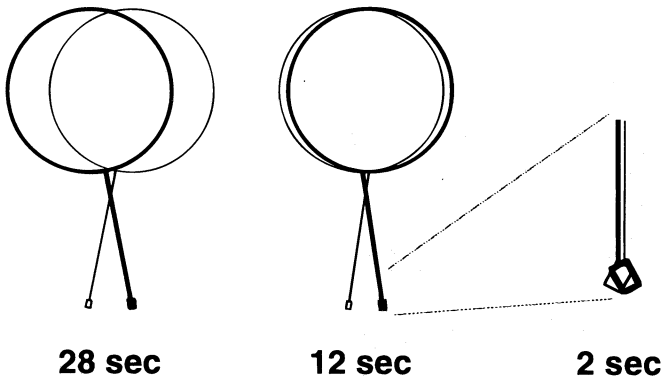

FIG. 13.—Illustration of the three pendular modes of the balloon/gondola system. Displacements are exaggerated.

The next lowest mode is one in which the gondola and flight train swing in one direction as the balloon rotates in the opposite direction. The calculated period for this mode is between 11 and 14 s, depending on the balloon-to-air coupling. In the early part of the flight an oscillation was observed with a period of 12 s, consistent with a 5% coupled air mass.

For the next mode, the gondola swings as the balloon and flight train rotate in the opposite direction. The calculated period for this mode is 2 s. The main uncertainty is the mass distribution of the gondola. There is an observed oscillation with a period of 2 s in the early part of the flight and after the gondola makes large motions (for example, when we made a 90° azimuth rotation to observe the Coma cluster).

We conclude that the three detected frequencies are manifestations of the three predicted modes and that other possible modes either are not excited or are quickly damped. These effects are visible only after wind-driven excitation during ascent and after a major slew of the telescope (e.g., to locate a calibration source). Their amplitudes immediately after such excitation are $\sim 10'$, but they damp out on timescales of 10 minutes and do not affect telescope pointing during the data-taking portions of the flight.

We also detect altitude oscillations of the balloon with characteristic periods of ~ 5 minutes. The amplitude is ~ 100 m, as determined by pressure sensors and Global Positioning System data. The peak in the power spectrum of this motion is broad, and the motion is intermittent.

4. THERMAL CONSIDERATIONS

The temperature of the ambient optical surfaces is a critical issue, since these surfaces contribute a significant amount of the total power seen by the detectors ($\sim 50\%$ in the lowest frequency channel, increasing to $\gtrsim 90\%$ for the highest frequency channel). Numerous temperature sensors are included to monitor critical components for correlating with the final data. Most of the optical surfaces are close to the ambient temperature because the MSAM flights are single night flights. Significant thermal perturbations are encountered as the Sun rises.

For ambient components, Analog Devices AD590 temperature sensors are used to measure their temperature to 0.1 K with an absolute accuracy of ~ 1 K. These thermometers are glued onto the back surface of the mirrors and other locations on the shield and gondola (see Fig. 7). There are 10 thermometers on the primary mirror, 2 on the secondary mirror, 4 on the ground shield, and 12 in other locations on the gondola frame. One thermometer (elevation motor temperature) failed at launch for MSAM1-92, and one thermometer on the secondary mirror failed on ascent for MSAM1-94, probably because of ground shield deformations interfering with the wiring.

Float altitude for the balloon is ~ 38 km, where the air temperature is ~ 235 K. The minimum temperature during ascent occurs at the tropopause (~ 18 km), where it is 215 ± 2 K. Since the pressure is low (2.25 torr or 300 Pa), equilibration to the ambient temperature happens slowly, especially for massive objects like the primary mirror and the gondola frame.

The primary mirror starts the flight at the ground temperature and is cooled as the gondola ascends. Cooling is assisted by the 6 ± 2 m s^{-1} downward wind during the ascent. The cooling is faster on the more exposed top half of the mirror than on the bottom half. At float altitude this cooling slows, and it does not come to full equilibrium even after 6 hours (see Fig. 14). During the observation period, the cooling rate is roughly uniform at 1.25 K hr^{-1}. The temperature gradients diminish much faster, the longest time constant being ~ 30 minutes for the smooth gradient over the whole mirror. More complex patterns have shorter time constants.

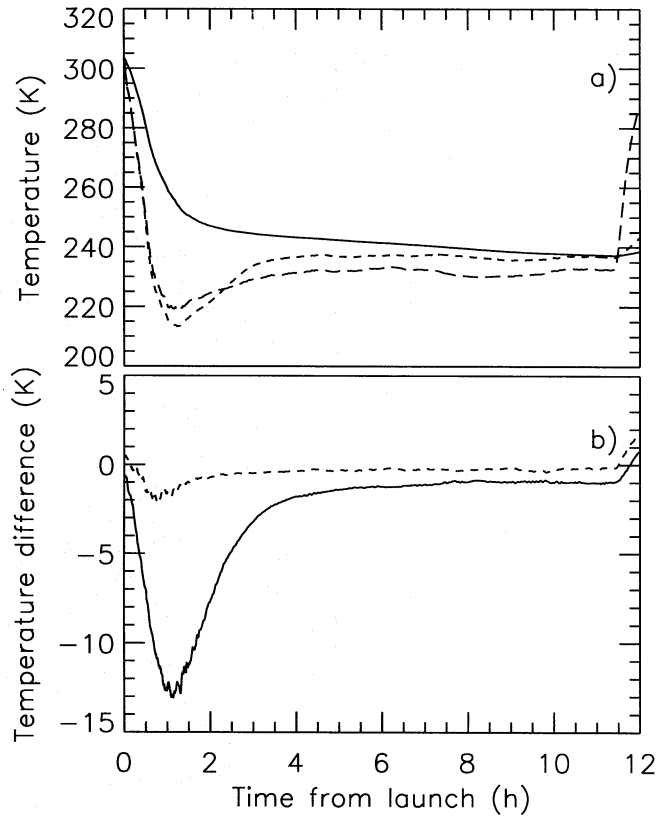

FIG. 14.—(*a*) Temperature of the primary mirror (*solid line*), secondary mirror (*dashed line*), and shield (*long-dashed line*). The kinks at 11.4 hr are caused by sunrise. (*b*) The temperature difference between the primary mirror bottom and top (*solid line*) shows the cooling effect of the ascent and the warming effect of the Sun on the top. The side-to-side difference in primary mirror temperature (*dashed line*) shows much smaller effects. The zeros in both (*a*) and (*b*) have not been calibrated and may be in error by ~ 0.5 K. The absolute temperature data in (*a*) have a resolution of 0.1 K. The temperature-difference data in (*b*) have a resolution of 1 mK. During a typical flight, CMBR data are not taken until 3 hr after launch.

© American Astronomical Society • Provided by the NASA Astrophysics Data System

1996ApJ...470...63F

The temperature of the primary mirror is critical, since even the 0.5% emissivity of good aluminum surfaces radiates more power than the CMBR in our lower frequency bands, and much more in the two higher bands. For anisotropy measurements, only the variation (both in time and in position) is potentially harmful to the experiment, but the required sensitivity is 5 orders of magnitude below the total power. There are two different effects to consider, one involving a uniform temperature and a varying emissivity over the mirror surface, and the other involving a nonuniform temperature.

Assuming a uniform temperature over the mirror but conservative, 10% variations in the emissivity ($\sim$0.05% changes in total emissivity) gives signals of order 120 mK. These signals are averaged over large sections of the mirror, and $\sim$90% of the area observed is the same in all three beam positions. This will reduce the estimated signal to $\sim$1 mK, which is the expected offset. In fact, in MSAM1-94, we see a very stable offset that is between 1 and 6 mK, depending on channel. The excess seems to be due to one of the positions of the secondary mirrors reflecting part of the gondola into the detectors. The temperature of the mirror changes by only 8 K over the observing time, which will produce a drift of 30 μK. Offset drifts slower than roughly 2.5 minutes are removed by a spline fit in the analysis, reducing this effect in the final data to below our sensitivity limit.

Assuming a uniform emissivity of 0.5%, but a 1 K temperature gradient across the mirror (the largest seen during the CMBR observations), gives a potential signal of 4 mK. This signal diminishes with a characteristic time of 30 minutes. The observation strategy repeats the scans every minute, reducing the signal to 100 μK. Averaging scans reduces this further, and the result is again smaller than the observation noise. The exact amount of rejection depends on the ability of the drift-removal algorithm to separate the slow drift of the mirror cooling from the 1 minute scans of the telescope. Higher modes in the thermal structure of the primary mirror are less well attenuated, but the effects are smaller and the coupling to the beam is less efficient. Thus, these modes are estimated to have a smaller net effect.

Although the secondary mirror radiates as much power onto the detectors as the primary mirror, the coupling of this power into the modulated signal is not significant. The modulation of the emitted power is only $\sim$0.05% (from the geometric change in the size of the secondary mirror as seen by the detectors, and from the small modulation in emissivity due to a change in the angle of incidence). For a $\sim$0.5% emissivity of the mirror surface, the mirror will generate a $\sim$1 mK offset. Thus, even a 10 K change in the secondary mirror temperature will generate only a 25 μK change in the modulated signal before additional attenuation by the other two levels of modulation. The temperature of the secondary mirror during a flight is also more uniform than the primary mirror, as shown in Figure 14.

5. TELEMETRY AND COMMANDING

Monitoring and controlling the observations are done through a remote commanding and telemetry system. The NSBF supplies a package, called the consolidated instrument package (CIP), which is flown on the payload. The capabilities of this system are described in detail in the NSBF User's Manual (National Scientific Balloon Facility 1996). The CIP provides the experimenter with several telemetry channels of various bandwidths, the widest of which is 49.5 kHz. It provides two types of commanding: a channel for 16 bit digital words, at a rate of about 1 s^{-1}, and 80 discrete commands, each of which pulses an individual line on the CIP, which can be sent at a rate of about 2 s^{-1}.

The telemetry and command layout of this instrument reflects its origin as two separate experiments. To integrate the systems as easily as possible, we have largely preserved their original telemetry and commanding interfaces. As a result, we use the commanding systems of two CIPs (but the telemetry transmitter of only one). Figure 15 shows a diagram of the MSAM1 telemetry and commanding systems.

In the various configurations for the three flights this instrument uses three or four telemetry channels. The system that controls the pointing of the gondola produces a biphase stream that includes information about the pointing sensors and actuators and the state of the controlling programs. This stream has a bit rate of 20.48 kHz. The system that controls the detectors produces a biphase stream at 4.096 kHz, including the detector data and information about the cryostat, chopper, etc. Finally, the camera systems produce telemetry containing information about star locations. The old camera system, which was flown on the first two flights, produced intermittent biphase packets at 800 Hz. The new camera system, which was flown on the second and third flights, produced an RS-232 stream at 4800 baud.

The digital word channel of one CIP communicates with the detector system. Each transmission sets one of 16 registers in the detector system; the high-order 4 bits select which register, and the low-order 12 bits specify the value to be set. These registers control, e.g., detector preamplifier gains and lock-in phase shifts.

The digital word channel of the other CIP communicates with the pointing system and the camera systems. These systems use a packet of words to specify each command. The packet encodes which subsystem the command is directed to, the action to be performed, any parameters needed to specify the action, and framing and length information.

The relay commands of the CIPs are used primarily for turning on and off latching relays. Relays are used to control batteries and power supplies, and to turn on and off various parts of the instrument, e.g., the liquid helium level sensor in the cryostat and the telescope balance pumps.

Neither the commanding nor the telemetry channels of the CIP are reliable in the communication theoretical sense; in other words, the system as supplied does not detect transmission failures and automatically resend. Typical failures are the following:

1. Dropouts in the telemetry channels, usually for a fraction of a second.
2. Failure of relay commands to arrive.
3. Digital word failing to arrive, or arriving altered.

In some cases, transmission can be quite poor, particularly for sending commands. Our experience with this has impressed upon us the necessity of keeping the length of command packets as short as possible, and adding automatic detection and retry of transmission failures.

The unreliable nature of the relay commands is easily dealt with by a general design rule: make the effect of sending a relay command twice the same as that of sending

© American Astronomical Society • Provided by the NASA Astrophysics Data System

1996ApJ...470...63F

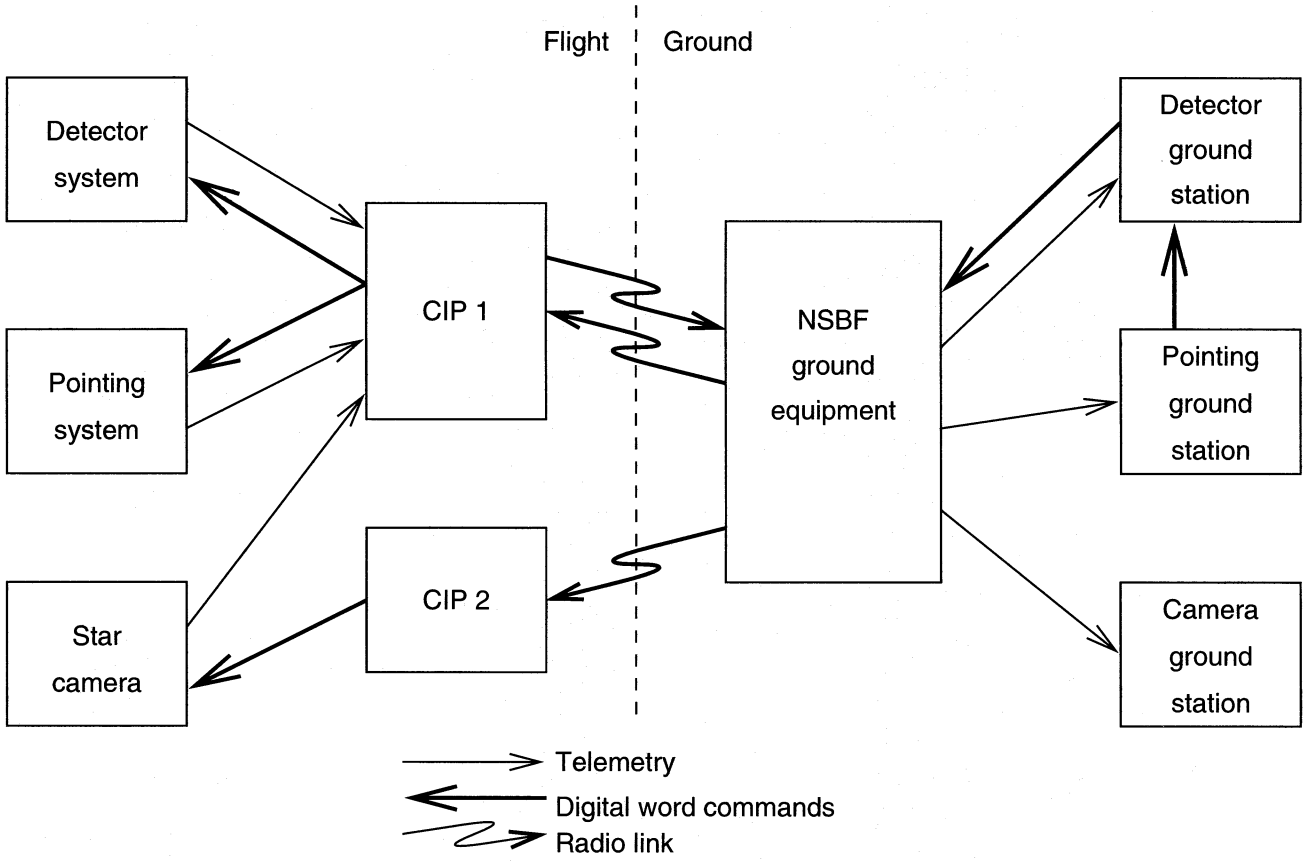

FIG. 15.—Block diagram of the command and telemetry system. The discrete commands are not shown; they follow the same paths as the digital word commands. The blocks with the lighter boundaries represent NSBF supplied equipment.

it once. For example, if a relay command is used to turn on a particular relay, then sending the command twice also has the effect of turning on the relay. Then, for critical commands, one adopts a practice of sending the command several times. Note that "toggling" type commands are strictly avoided.

We partially compensate for noise and dropouts in the telemetry downlink by using an error detection and correction scheme. For the radiometer data stream, a hardware ECC generator (designed for computer storage disk subsystems) encodes the redundant information. Software in the ground system performs error correction where possible and, at a minimum, flags unreliable data. For a normal flight with typical telemetry quality, this system corrects several hundreds of telemetry errors per flight, and flags on the order of 100 uncorrectable errors.

6. POWER AND WEIGHT

The power systems for the radiometer and the gondola are also independent. Radiometer electronics and heater power is supplied by two 32 V lithium SDX battery packs (model B7901-12 from Eternacell, Inc.) supplied by the NSBF. These are augmented by six 15 V packs (model B9525) for several small motors and relays. A PowerCube, Inc. modular DC-DC converter (part No. XDD1784) is used to generate the supply voltages and has a primary conversion frequency of ~ 30 kHz. Because of the potential sensitivity of the detectors to high-frequency power, the supply voltages for the detector preamplifiers and the bias lines for the detectors have an additional level of regulation from a set of linear regulators, and are then heavily filtered. We have not been able to measure any undesirable effects from using the DC-DC power converters in this way. During ground testing where the batteries are replaced by high-current DC-DC power supplies, a small effect at the conversion frequency of 18 kHz can be measured on the preamplifier power lines. This noise is attributed to some unavoidable ground currents and is not present in the flight configuration.

Gondola power is provided by 15 sets of 32 V model B7901-12 packs. Eight of these are used for the motors. We have sized the battery capacity for the maximum current draw of the motors, resulting in a capacity that is 4 times the average over an entire flight. The gondola electronics uses seven additional packs, and powers the gondola command, control, telemetry, and star camera functions.

Secondary gondola voltages are generated by a set of Vicor DC-DC converters whose chopping frequencies are not detectable in the radiometer output signals. All power supply clocks operate at random phase with respect to the chopped optical signal.

Table 3 summarizes the overall weight and power budgets for the instrument. The reduction in weight of the gondola frame and jitter mechanism after MSAM1-92 is a result of switching to the cable top structure. The gondola electronics weight changes as we upgrade various subsystems. The star camera weight increased for MSAM1-94 because we flew both the old CID and the new CCD

© American Astronomical Society • Provided by the NASA Astrophysics Data System

1996ApJ...470...63F

TABLE 3

SUMMARY OF WEIGHTS AND POWER

Item	MSAM1-92 Weight (kg)	MSAM1-94 Weight (kg)	MSAM1-95 Weight (kg)	Power Consumption (W)
Primary mirror	75	75	75	...
Secondary mirror	8	8	8	30
Ground shield	50	15	15	...
Cryostat/detectors	105	105	105	0.1
Strongback	140	140	140	...
Primary gyro	15	15	15	36
Secondary gyro	10	...	10	48
Elevation mechanism	66	66	66	80
Azimuth mechanism	110	110	110	40
Fluid mechanism	20	20	20	10
Jitter mechanism	55	20	20	28
Radiometer electronics	45	45	45	90
Gondola electronics	30	40	40	120
Camera and electronics	16	26	10	20
Power conditioning	15	15	15	80
Batteries	110	120	130	...[a]
Frame	450	380	380	...
Telemetry (NSBF)	50	85	85	...[b]
Lead bricks	50	60	30	...
Ballast	320	320	320	...
Crush pads	40	40	40	...
Miscellaneous	100	105	91	...
Total	1880	1810	1770	585

[a] The batteries supply 20 kW hr.

[b] Power for telemetry transmission supplied by an internal lithium battery in the CIP.

cameras. We increased the battery complement for each flight in order to accommodate tests for new subsystems.

7. CONCLUSIONS

The telescope and gondola we describe has supported the three MSAM1 flights over the past four years. The accuracy and stability of the platform simplify operational procedures and aid in data collection and analysis. The reliability of this 15 year old gondola was initially a concern, but by upgrading a small number of selected subsystems, performance has been maintained, and in some cases improved. At most, 1–2 hr of flight time were lost (out of almost 40 hr) as a result of gondola-related anomalies. Most of this loss resulted from difficulties with the command link.

The optical performance after the improvement in the gondola superstructure is verified to be adequate for the measurements. However, the sensitivity of CMBR measurements to earthshine continues to be an area of concern because of the difficulty of providing adequate shielding and the concomitant validation measurements. The method we have described for mapping the sidelobe performance of the gondola is strongly recommended for all similar payloads to help alleviate some of these concerns.

We would like to thank the staff of the National Scientific Balloon Facility in Palestine, Texas, for continuing to make ballooning a satisfying and productive experimental activity. In particular, for this project they took on an increased burden by agreeing to provide two CIPs for our package so that we can carry out the measurements with a minimum of electronic changes to the gondola and radiometer. The National Aeronautics and Space Administration supports this research through grants NAGW 1841, RTOP 188-44, NGT 50908, and NGT 50720.

REFERENCES

Bennett, C. L., et al. 1994, ApJ, 436, 423
Cheng, E. S. 1994, in Present and Future of the Cosmic Microwave Background, ed. J. L. Sanz et al. (Lecture Notes in Physics, Vol. 429; New York: Springer), 76
Cheng, E. S., et al. 1994, ApJ, 422, L37
———. 1996, ApJ, 456, L71
de Bernardis, P., et al. 1994, ApJ, 422, L33
Downey, P. M., et al. 1984, Appl. Opt., 23, 910
Fischer, M. L., et al. 1992, ApJ, 388, 242
Ganga, K., Cheng, E., Meyer, S., & Page, L. 1993, ApJ, 410, L57
Ganga, K., Page, L., Cheng, E., & Meyer, S. 1994, ApJ, 432, L15
Hauser, M. G., et al. 1984, ApJ, 285, 74
Hazen, N. L. 1974, in Proc. SPIE, 44, 41
Hazen, N. L., Coyle, L. M., & Diamond, S. M. 1974, in Telescope Systems for Balloon-borne Research, ed. C. Swift et al. (Moffett Field: NASA/ARC), 202
Inman, C. A., et al. 1996, ApJ, submitted (preprint astro-ph/9603017)
Kowitt, M. S., et al. 1995, Astrophys. Lett. Commun., 32, 273
———. 1996, ApJ, submitted (preprint astro-ph/9604155)
Meinhold, P. R., Chingcuanco, A. O., Gundersen, J. O., Schuster, J. A., Seiffert, M. D., Lubin, P. M., Morris, D., & Villela, T. 1993, ApJ, 406, 12
Meyer, S. S., Cheng, E. S., & Page, L. A. 1991, ApJ, 371, L7
National Scientific Balloon Facility. 1996, NSBF User's Manual (available from NSBF, Palestine, TX)
Page, L. A. 1989, Ph.D. thesis, MIT
Page, L. A., Cheng, E. S., Golubovic, B., Gundersen, J., & Meyer, S. S. 1994, Appl. Opt., 33, 11
Page, L. A., Cheng, E. S., & Meyer, S. S. 1990, ApJ, 355, L1
White, M., Scott, D., & Silk, J. 1994, ARA&A, 32, 319

© American Astronomical Society • Provided by the NASA Astrophysics Data System